

Supplement of Earth Surf. Dynam., 6, 121–140, 2018
<https://doi.org/10.5194/esurf-6-121-2018-supplement>
© Author(s) 2018. This work is distributed under
the Creative Commons Attribution 4.0 License.



Supplement of

U–Th and ¹⁰Be constraints on sediment recycling in proglacial settings, Lago Buenos Aires, Patagonia

Antoine Cogez et al.

Correspondence to: Antoine Cogez (antoine.cogez@gmail.com)

The copyright of individual parts of the supplement might differ from the CC BY 4.0 License.

1 U-Th series disequilibria and the determination of time constant for weathering

The nuclides of the U-series have been recognized since the 1960s as powerful tools to constrain the time constants of the weathering and erosion processes (e.g. Rosholt et al., 1966; Hansen & Stout, 1968). Such a potential was convincingly illustrated from the 2000s by case studies, as well for the determination of time constants of weathering processes, as for time constants of sedimentary transfers in alluvial plains. The theoretical principle behind these approaches can be found in Osmond & Ivanovich (1992); Chabaux et al. (2003b,a, 2008); Dosseto & Schaller (2016) to which we refer the reader for further details. It relies on the property of the radionuclides (1) to be fractionated during water rock interactions, which create what it is named radioactive disequilibria among the U-series nuclides, and (2) to have radioactive period of the same order of magnitude as the time constants of several weathering processes. The study of the variations of the ^{238}U - ^{234}U - ^{230}Th - ^{226}Ra radioactive disequilibria in soil and weathering profiles have thus allowed for bringing time constants of weathering processes (e.g. Dequincey et al., 2002; Chabaux et al., 2003a; Dosseto et al., 2008, 2012; Pelt et al., 2008; Ma et al., 2010, 2013; Ackerer et al., 2016). Similarly the variations of ^{238}U - ^{234}U - ^{230}Th - ^{226}Ra disequilibria in sediments along the river might be used to constrain the residence time of sediment within the alluvial plain (Granet et al., 2007, 2010) even if such an approach is still debated (Chabaux et al., 2012; Bosia et al., 2016, in press). For determining sediment residence and transfer time, an alternative approach the “comminution” age approach has been developed (DePaolo et al., 2006, 2012), that we detail in the article.

2 Specific surface area measurements

The specific surface areas S of the samples were measured using N_2 adsorption. S was calculated by determining the amount of adsorbed gas needed to create a monomolecular layer on the sample’s connected surface. Each sample was placed in a vacuum-sealed vessel (itself placed in a liquid nitrogen bath). First, a non-adsorbing gas (in this case, He) was introduced in pressure increments and the injected volume V_{na} was recorded. After having removed the gas, a second series of gas injections was run with an adsorbing gas (in this case N_2) and the volume V_a recorded. The volume of gas adsorbed on the surface of the sample at each pressure increment is therefore $V_a - V_{na}$. Assuming that the surface of the sample interacts with a monomolecular layer of adsorbed gas (following the BET theory, Brunauer et al. (1938)), the volume of this

layer, V_m , is derived as a function of $V_a - V_{na}$, valid for pressures between 0.05 and 0.35 of the N_2 saturated vapour pressure. Specific surface area is calculated as:

$$S = \frac{V_m \cdot A \cdot N_a}{m \cdot V_{STP}} \lambda_{230} N_{230} + (1 - f_\alpha^{230}) \lambda_{234} N_{234} \quad (1)$$

where N_a is Avogadro's constant, A is the adsorption cross-sectional area of the adsorbing gas molecule, m is the mass of the dry sample, and V_{STP} is the volume of one mole of adsorbed gas at standard pressure and temperature.

3 Determination of profiles ^{10}Be ages

We show here graphically (Figures 1 and 2) the results of the Monte Carlo optimization of the profiles ages, erosion rates, and inheritance, following Hidy et al. (2010). Monte Carlo optimization allow the determination of the best set of values for erosion rates of the surface, deposition age, and nuclides inheritance, to best explain the profiles of ^{10}Be concentrations. A priori values for these three parameters are assigned (see section 2.2.3). This is a probabilistic approach, so the result is shown in term of probability distribution.

4 Th removal during leaching

Th is poorly soluble, hence after ejection by α recoil, it is most probably readsorbed onto mineral surfaces. The leaching protocol is supposed to remove it. In order to evaluate whether the leaching procedure has been efficient at removing exchangeable Th, we test whether the results are compatible with scenarios where Th is not removed or only partially removed.

To test it, we consider that a total readsorption of ^{230}Th after ejection from the mineral is equivalent to no ejections at all, that is $f_\alpha^{230} = 0$. We also test with $f_\alpha^{230} = \frac{1.176 \times f_\alpha^{234}}{2}$ (half of the theoretical value described in section 2.3.1), which correspond to an intermediate case (partial removal of Th during leachings).

Interestingly the relations between t_{recycl} and $k_{238}^{pre}/k_{238}^{post}$ remain the same. The differences concern the likelihood of the solutions, and the relation between k_{234}/k_{238} and k_{230}/k_{238} (see Figures 3 and 4). With $f_\alpha^{230} = 0$, the fit to the data is poor and unrealistic values of k_{234}/k_{238} larger than 3 are necessary. When f_α^{230} is increased, the predicted value of k_{234}/k_{238} decreases, but remains larger than 3, the fit to the data becomes better, and the t_{recycl} optimal solution

remains around 100 kyrs.

Given the fact that the fit to the data is less good and the estimated value of k_{234}/k_{238} becomes very large as the value of f_{α}^{230} is decreased, we conclude that the leaching procedure is highly efficient at removing exchangeable Th, even if we cannot exclude that a small amount of exchangeable Th can remain after the leaching protocol. Importantly, the average recycling time estimated from the inverse procedure remains of the order of 100 kyrs, even with moderate amounts of Th.

References

References

- Ackerer, J., Chabaux, F., Van der Woerd, J., Viville, D., Pelt, E., Kali, E., Lerouge, C., Ackerer, P., di Chiara Roupert, R., & Négrel, P. (2016). Regolith evolution on the millennial timescale from combined u–th–ra isotopes and in situ cosmogenic ^{10}Be analysis in a weathering profile (strengbach catchment, france). *Earth and Planetary Science Letters*, *453*, 33–43.
- Bosia, C., Chabaux, F., Pelt, E., Cogez, A., Stille, P., Deloule, E., & France-Lanord, C. (in press). U-series disequilibria in minerals from gandak river sediments (himalaya). *Chemical Geology*, .
- Bosia, C., Chabaux, F., Pelt, E., France-Lanord, C., Morin, G., Lavé, J., & Stille, P. (2016). U–th–ra variations in himalayan river sediments (gandak river, india): Weathering fractionation and/or grain-size sorting? *Geochimica et Cosmochimica Acta*, *193*, 176–196.
- Brunauer, S., Emmet, P., & Teller, F. (1938). Surface area measurements of activated carbons, silica gel and other adsorbents. *J. Am. Chem. Soc.*, *60*, 309–319.
- Chabaux, F., Blaes, E., Granet, M., di Chiara Roupert, R., & Stille, P. (2012). Determination of transfer time for sediments in alluvial plains using ^{238}U – ^{234}U – ^{230}Th disequilibria: The case of the ganges river system. *Comptes Rendus Geoscience*, *344*, 688–703.
- Chabaux, F., Bourdon, B., & Riotte, J. (2008). U-series geochemistry in weathering profiles, river waters and lakes. *Radioactivity in the Environment*, *13*, 49–104.
- Chabaux, F., Dequincey, O., Lévêque, J., Leprun, J., Clauer, N., Riotte, J., & Paquet, H. (2003a). Tracing and dating recent chemical transfers in weathering profiles by trace-element geochemistry and ^{238}U – ^{234}U – ^{230}Th disequilibria: the example of the kaya lateritic toposequence (burkina-faso). *Comptes Rendus Geoscience*, *335*, 1219–1231.
- Chabaux, F., Riotte, J., & Dequincey, O. (2003b). U–th–ra fractionation during weathering and river transport. *Reviews in Mineralogy and Geochemistry*, *52*, 533–576.
- DePaolo, D., Maher, K., Christensen, J., & McManus, J. (2006). Sediment transport time measured with u-series isotopes: results from odp north atlantic drift site 984. *Earth and Planetary Science Letters*, *248*, 394–410.

-
- DePaolo, D. J., Lee, V. E., Christensen, J. N., & Maher, K. (2012). Uranium comminution ages: Sediment transport and deposition time scales. *Comptes Rendus Geoscience*, *344*, 678–687.
- Dequincey, O., Chabaux, F., Clauer, N., Sigmarsson, O., Liewig, N., & Leprun, J.-C. (2002). Chemical mobilizations in laterites: evidence from trace elements and ^{238}U - ^{234}U - ^{230}Th disequilibria. *Geochimica et Cosmochimica Acta*, *66*, 1197–1210.
- Dosseto, A., Bourdon, B., & Turner, S. P. (2008). Uranium-series isotopes in river materials: insights into the timescales of erosion and sediment transport. *Earth and Planetary Science Letters*, *265*, 1–17.
- Dosseto, A., Buss, H., & Suresh, P. (2012). Rapid regolith formation over volcanic bedrock and implications for landscape evolution. *Earth and Planetary Science Letters*, *337*, 47–55.
- Dosseto, A., & Schaller, M. (2016). The erosion response to quaternary climate change quantified using uranium isotopes and in situ-produced cosmogenic nuclides. *Earth-Science Reviews*, *155*, 60–81.
- Granet, M., Chabaux, F., Stille, P., Dosseto, A., France-Lanord, C., & Blaes, E. (2010). U-series disequilibria in suspended river sediments and implication for sediment transfer time in alluvial plains: the case of the himalayan rivers. *Geochimica et Cosmochimica Acta*, *74*, 2851–2865.
- Granet, M., Chabaux, F., Stille, P., France-Lanord, C., & Pelt, E. (2007). Time-scales of sedimentary transfer and weathering processes from u-series nuclides: clues from the himalayan rivers. *Earth and Planetary Science Letters*, *261*, 389–406.
- Hansen, R., & Stout, P. (1968). Isotopic distributions of uranium and thorium in soils.
- Hidy, A., Gosse, J., Pederson, J., Mattern, J., & Finkel, R. (2010). A geologically constrained monte carlo approach to modeling exposure ages from profiles of cosmogenic nuclides: An example from lees ferry, arizona. *Geochemistry, Geophysics, Geosystems*, *11*.
- Ma, L., Chabaux, F., Pelt, E., Blaes, E., Jin, L., & Brantley, S. (2010). Regolith production rates calculated with uranium-series isotopes at susquehanna/shale hills critical zone observatory. *Earth and Planetary Science Letters*, *297*, 211–225.
- Ma, L., Chabaux, F., West, N., Kirby, E., Jin, L., & Brantley, S. (2013). Regolith production and transport in the susquehanna shale hills critical zone observatory, part 1: Insights from u-series isotopes. *Journal of Geophysical Research: Earth Surface*, *118*, 722–740.

-
- Osmond, J., & Ivanovich, M. (1992). Uranium-series mobilization and surface hydrology. In *Uranium-series disequilibrium: applications to earth, marine, and environmental sciences*. 2. ed.
- Pelt, E., Chabaux, F., Innocent, C., Navarre-Sitchler, A., Sak, P. B., & Brantley, S. (2008). Uranium–thorium chronometry of weathering rinds: rock alteration rate and paleo-isotopic record of weathering fluids. *Earth and Planetary Science Letters*, 276, 98–105.
- Rosholt, J., Doe, B., & Tatsumoto, M. (1966). Evolution of the isotopic composition of uranium and thorium in soil profiles. *Geological Society of America Bulletin*, 77, 987–1004.

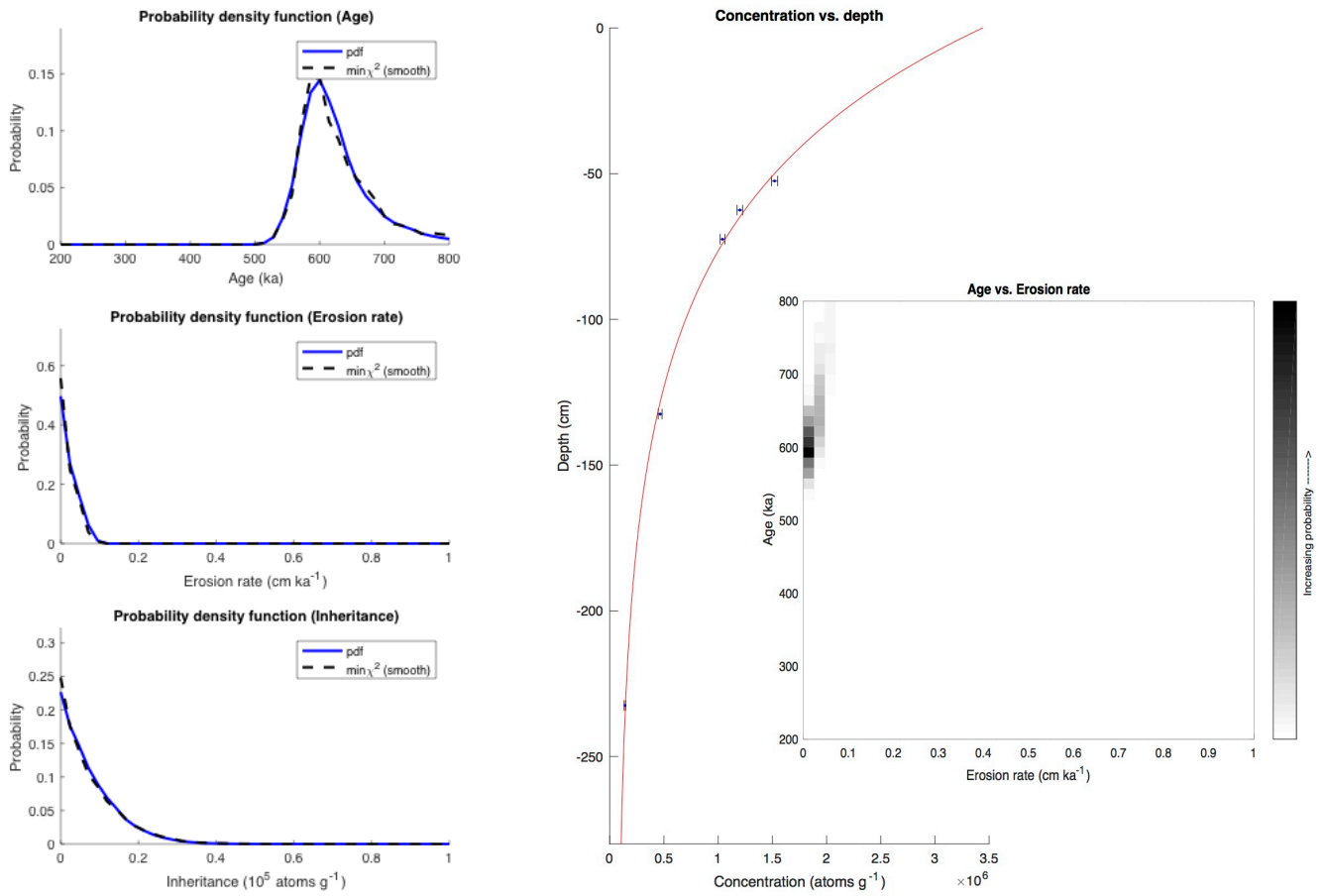


Figure 1: (Left panel) Distribution of the optimal solutions for age, erosion rate, and inheritance for the inversion of Deseado 2 profile ¹⁰Be data. (Right panel) The optimal model of ¹⁰Be versus depth, resulting from the set of optimal age, erosion rate and inheritance. The probability of erosion rates and ages is also plotted in a two dimensional diagram. These figures have been drawn from the matlab code supplied by Hidy et al. (2010).

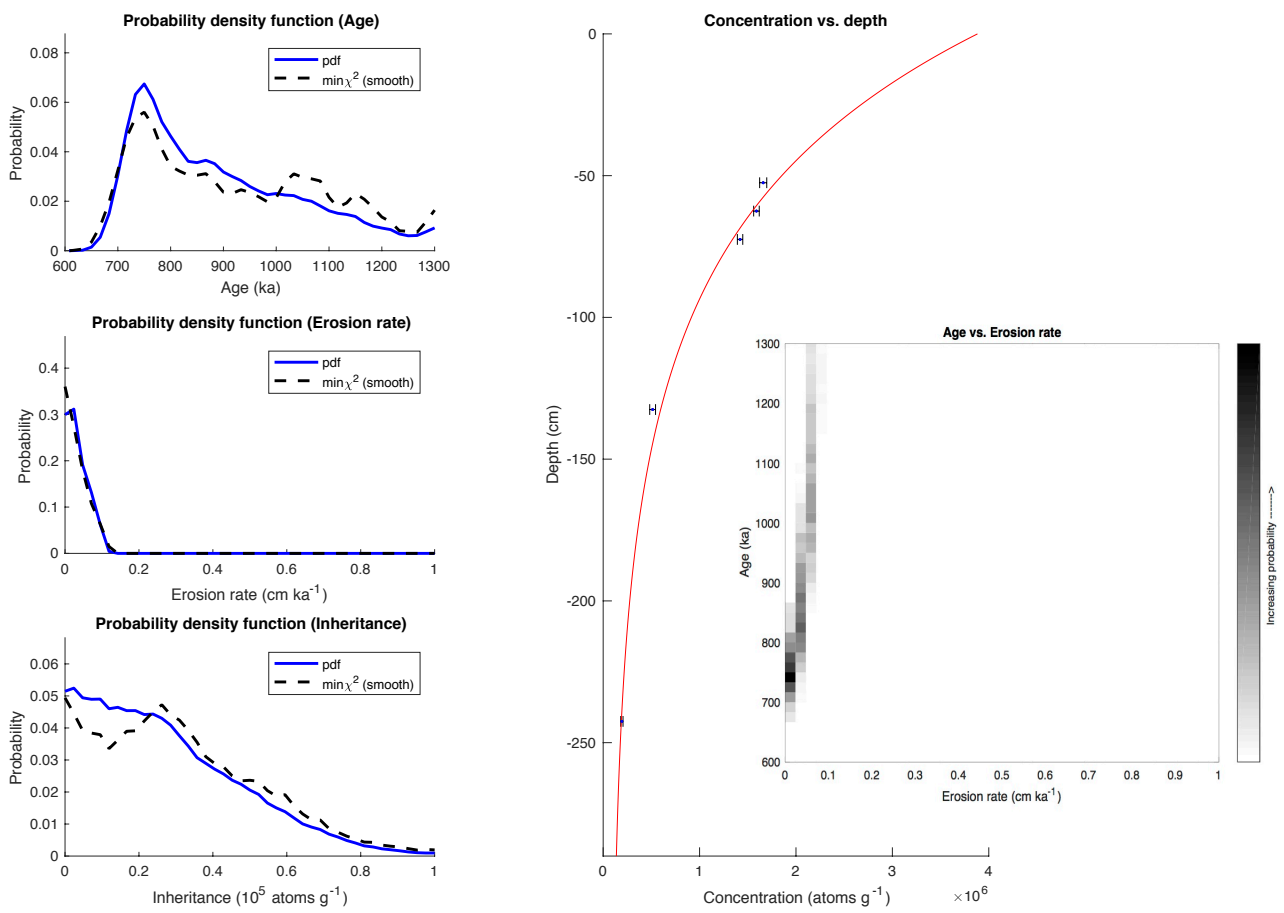


Figure 2: Same as Figure 1 for the Telken 5 profile.

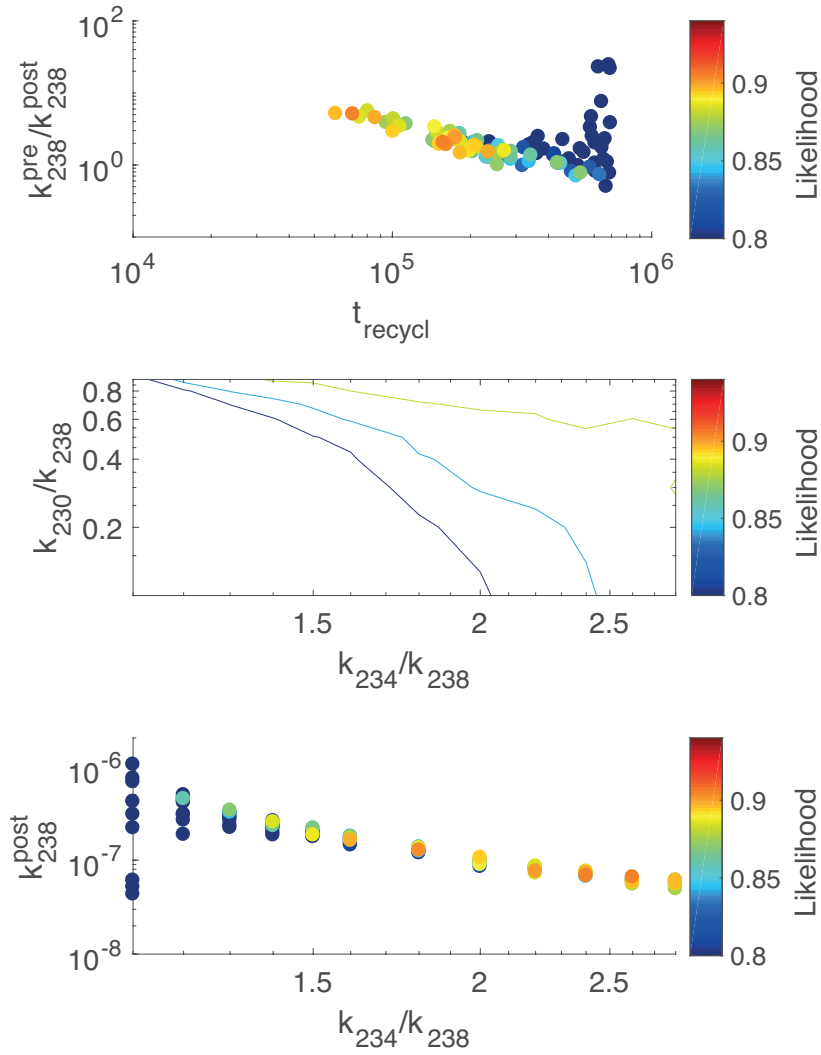


Figure 3: Results of Monte Carlo simulation with $f_{\alpha}^{230} = 0$. This case means that ^{230}Th is not removed from the mineral grains by α -recoil. Note that for readability the colorscale has been changed compared to Figure 6.

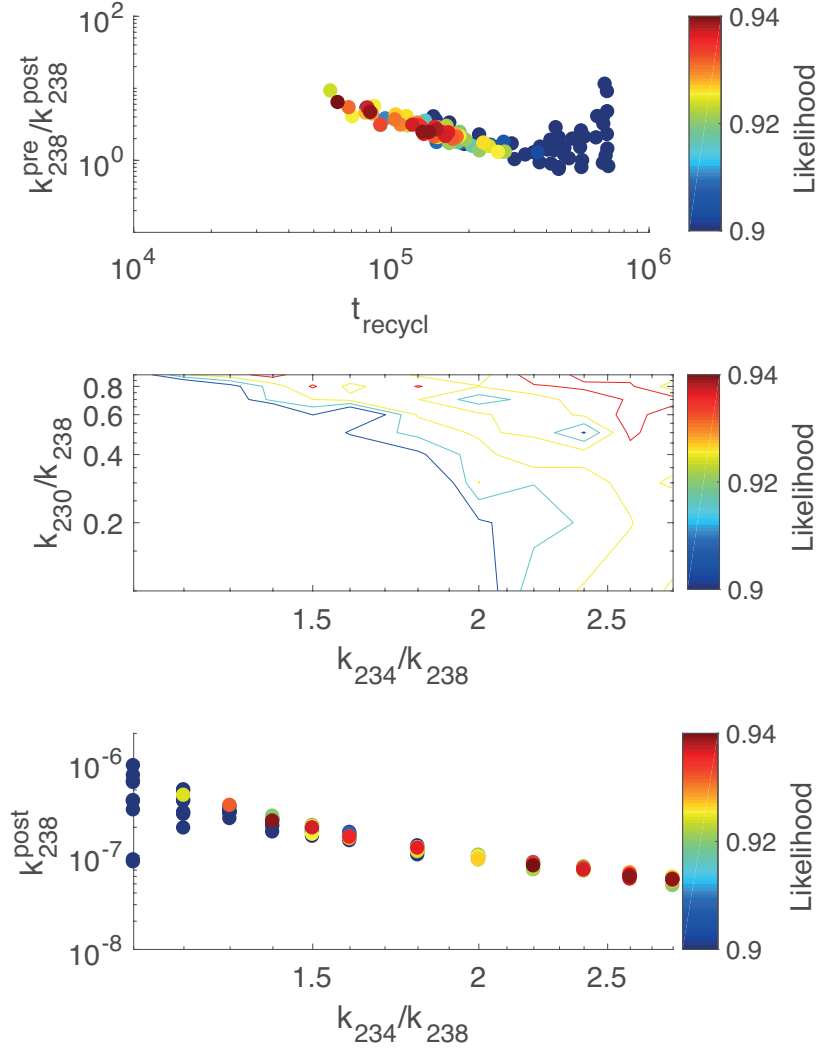


Figure 4: Results of Monte Carlo simulation with $f_{\alpha}^{230} = \frac{1.176 \times f_{\alpha}^{234}}{2}$ (half of the theoretical value described in section 2.3.1). The colorscale is the same as in Figure 6.

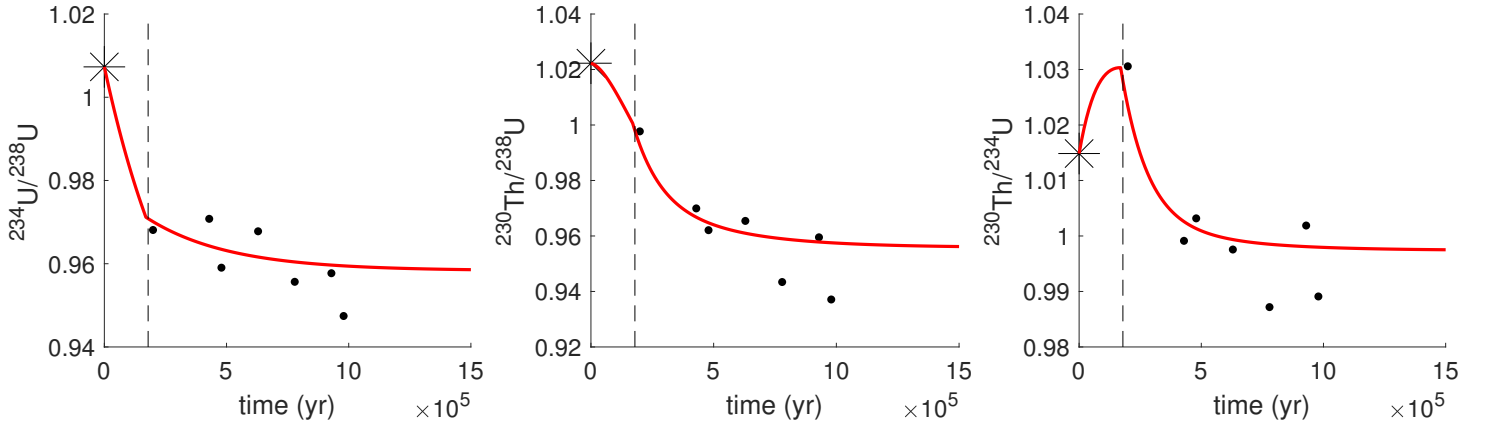


Figure 5: Best fit of the Monte Carlo simulation (red curves). The black points are the data. The X axis originate in the comminution episode, which means that the age assigned to each sample is the addition of its ¹⁰Be exposure age and the recycling time (determined with U-Th data). Errorbars are the external uncertainties. The black vertical dashed line shows the recycling time. This corresponds to a recycling time of 180 kyrs, a ratio $k_{238}^{pre}/k_{238}^{post} = 2.35$, $k_{234}/k_{238} = 1.4$, and $k_{230}/k_{238} = 0.6$.

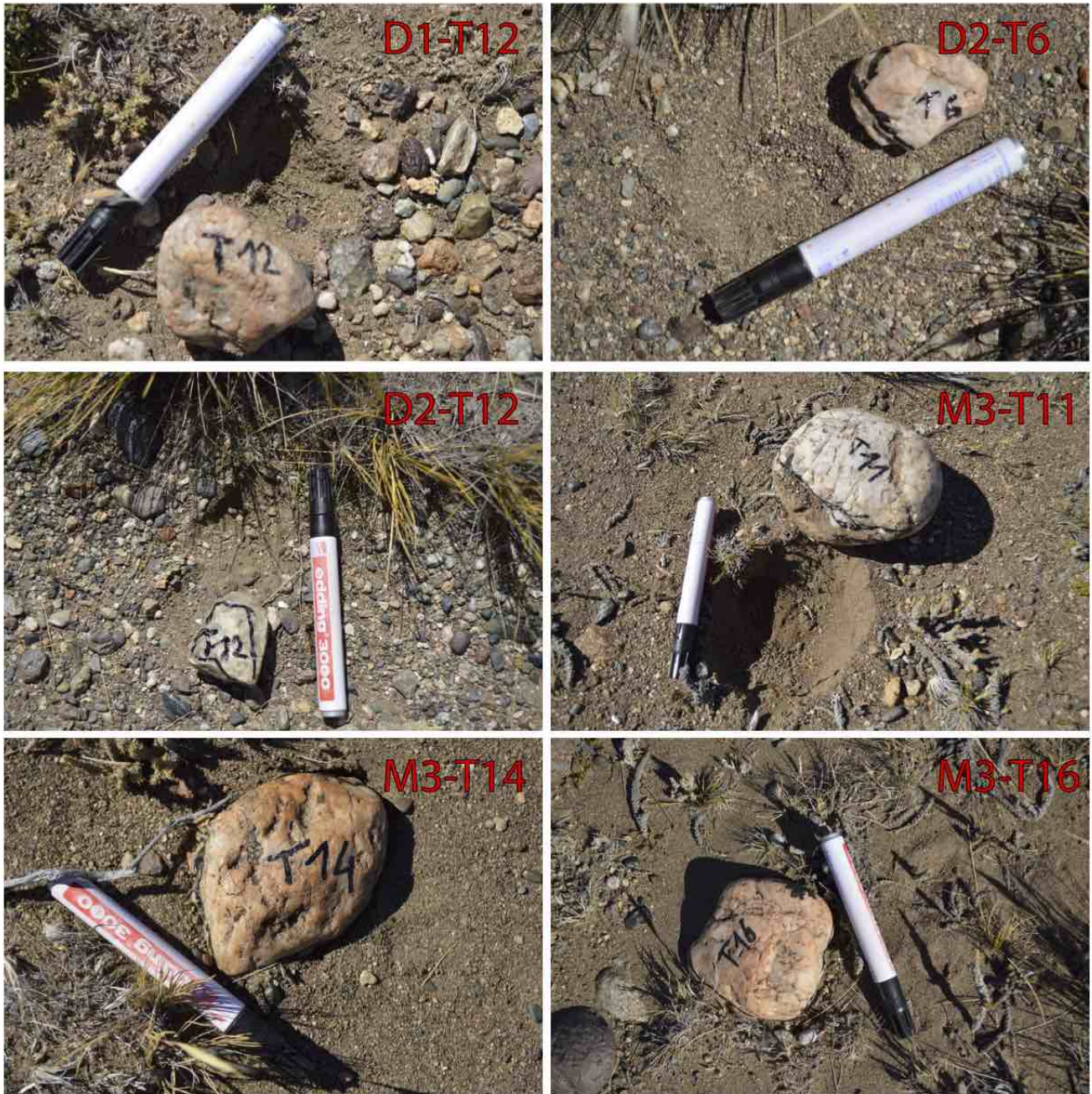


Figure 6: Pictures of a few cobbles sampled on the field. For each picture, the cobble had been removed from its place and the imprint is still visible.

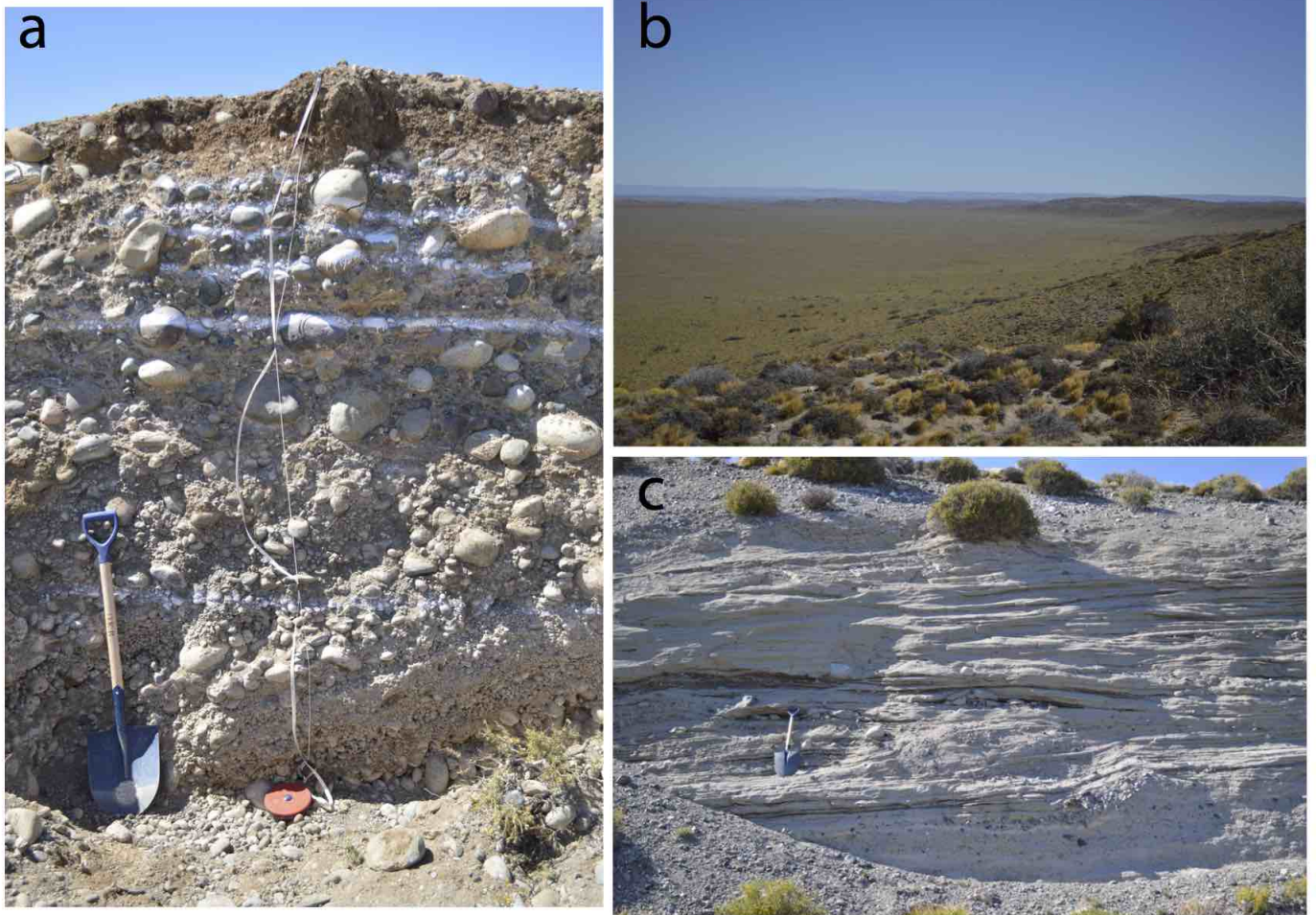


Figure 7: [a] Pictures of the Telken 5 profile. Each white line represent the level on which the samples have been taken. [b] Picture showing the Moreno 1 moraine above the Fenix outwash. In the back we see the older moraines at higher elevation. [c] Example of the kind of outcrops in the moraines, in which the silt sample were taken. Fine silty beds within the moraine, far from the moraine surface.